

# Transmission of photonic quantum polarization entanglement in a nanoscale hybrid plasmonic waveguide

Ming Li,<sup>†,‡,§</sup> Chang-Ling Zou,<sup>†,‡,§</sup> Xi-Feng Ren,<sup>\*,†,‡</sup> Xiao Xiong,<sup>†,‡</sup> Yong-Jing Cai,<sup>†,‡</sup> Guo-Ping Guo,<sup>†,‡</sup> Li-Min Tong,<sup>¶</sup> and Guang-Can Guo<sup>†,‡</sup>

*Key Laboratory of Quantum Information, University of Science and Technology of China, CAS, Hefei, 230026, People's Republic of China, Synergetic Innovation Center of Quantum Information & Quantum Physics, University of Science and Technology of China, Hefei, Anhui 230026, China, and State Key Laboratory of Modern Optical Instrumentation, Department of Optical Engineering, Zhejiang University, Hangzhou 310027, China*

E-mail: renxf@ustc.edu.cn

---

\*To whom correspondence should be addressed

<sup>†</sup>Key Laboratory of Quantum Information, University of Science and Technology of China, CAS, Hefei, 230026, People's Republic of China

<sup>‡</sup>Synergetic Innovation Center of Quantum Information & Quantum Physics, University of Science and Technology of China, Hefei, Anhui 230026, China

<sup>¶</sup>State Key Laboratory of Modern Optical Instrumentation, Department of Optical Engineering, Zhejiang University, Hangzhou 310027, China

<sup>§</sup>Contributed equally to this work

## Abstract

Photonic quantum technologies have been extensively studied in quantum information science, owing to the high-speed transmission and outstanding low-noise properties of photons. However, applications based on photonic entanglement are restricted due to the diffraction limit. In this work, we demonstrate for the first time the maintaining of quantum polarization entanglement in a nanoscale hybrid plasmonic waveguide composed of a fiber taper and a silver nanowire. The transmitted state throughout the waveguide has a fidelity of 0.932 with the maximally polarization entangled state  $\Phi^+$ . Furthermore, the Clauser, Horne, Shimony, and Holt (CHSH) inequality test performed, resulting in value of  $2.495 \pm 0.147 > 2$ , demonstrates the violation of the hidden variable model. Since the plasmonic waveguide confines the effective mode area to subwavelength scale, it can bridge nanophotonics and quantum optics, and may be used as near-field quantum probe in a quantum near-field micro/nano-scope, which can realize high spatial resolution, ultra-sensitive, fiber-integrated, and plasmon-enhanced detection.

## Keywords

Surface plasmon polaritons, Quantum entanglement, Silver nanowire

## Introduction

Quantum entanglement is one of the most extraordinary phenomena borne out of quantum theory,<sup>1</sup> and lies at the heart of quantum information and future quantum technologies. From a fundamental aspect, it is used to prove the Copenhagen interpretation of quantum mechanics, against the famous EPR paradox.<sup>2,3</sup> Quantum entanglement has powerful applications in information processing and communications, as well as in the enhanced precision of measurement.<sup>4</sup> Quantum metrology,<sup>4</sup> as an important application of quantum entanglement, is the measurement of physical parameters with enhanced resolution and sensitivity, enabled by taking advantage of quantum theory, particularly by

exploiting quantum entanglement. For example, phase measurement with super-sensitivity beyond the standard quantum limit (SQL) can be realized by using  $N$ -particles entangled state ( $N \geq 2$ ).<sup>5-8</sup> This has many important applications, including gravitational wave detection, measurements of distance and optical properties of materials, and chemical and biological sensing. Very recently, entanglement-enhanced microscopes, which give a signal-to-noise ratio better than that limited by the SQL,<sup>9,10</sup> have been realized. In these experiments, structures were measured using the far field method, and the entangled photons were focused by an objective lens onto the sample surface. Therefore, the spatial resolution of this type of optical imaging system was fundamentally limited by the well-known Abbe diffraction limit.

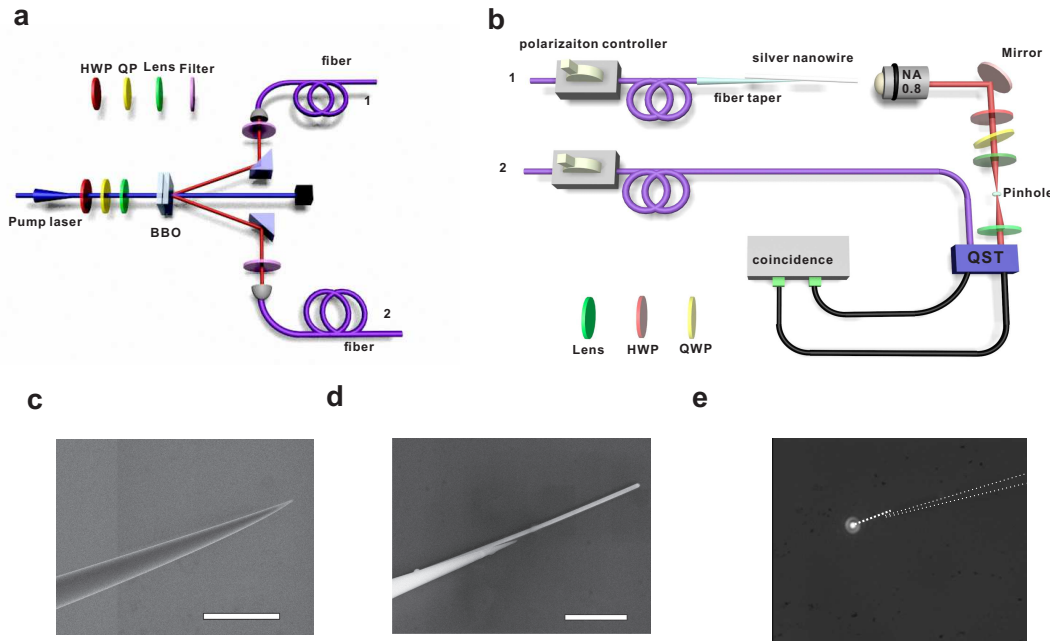


Figure 1: (color online) Experimental set-up. (a) The polarization entangled photon source generated by a degenerate type-I non-collinear spontaneous parametric down-conversion (SPDC) process. The produced photon pairs (808 nm) are separated in free space by a  $6^\circ$  angle based on the phase-matching condition and directed to different optical single-mode fibers. (b) One of the single mode fibers is connected with a tapered fiber or further coupled with a silver nanowire, output photons are collected by an objective lens and sent to the quantum state tomography (QST) apparatus, and the other fiber is directly connected to the QST. QP: Quartz plate; HWP: half-wave plate; QWP: quarter-wave plate; BBO:  $\beta - \text{BaB}_2\text{O}_4$ . (c) Scanning electron microscope (SEM) image of a tapered fiber with a tip radius of about 60 nm. Scale bar:  $5 \mu\text{m}$ . (d) SEM image of a fiber taper coupled with a 160 nm radius silver nanowire. Scale bar:  $5 \mu\text{m}$ . (e) CCD image of the hybrid waveguide. Laser light is guided through the fiber taper, then coupled to the silver nanowire and finally re-radiated from the nanowire end.

To overcome this limitation, near field optics, such as a near-field scanning optical microscope (NSOM), were developed. Typically, dielectric tips (silica taper or nano-aperture) are used to probe nano-structures beyond the diffraction limit. However, these near field probes suffer from ultralow transmittance, generally only about  $10^{-3}$ . An alternative method is to utilize surface plasmon polaritons (SPPs),<sup>11</sup> where the collective oscillations of free electrons are unlimited by the diffraction. Not only can SPPs confine light beyond the diffraction limit, but they can also enhance the light-matter interaction.<sup>12</sup> Among various plasmonic structures, silver nanowires are a natural choice for practical applications for several reasons: they are easy to prepare, have regular and uniform geometry, and undergo relatively low losses. Recently, great progress has been achieved in implementing silver nanowire photonics for various applications,<sup>13,14</sup> such as waveguides, compact logic gates, single-photon sources, nanoscale sensing and even single photon-level transistors.

Besides the studies on the classical applications of plasmonic structures, researchers have started to investigate plasmonics in the quantum regime. It has been experimentally proved that quantum polarization entanglement,<sup>15</sup> energy-time entanglement,<sup>16</sup> and orbital angular momentum entanglement<sup>17</sup> can be preserved in the photon-SPP-photon conversion process through metal hole arrays. But the metallic film thickness is less than optical diffraction limit (usually only about 100 nm), which limits its application in plasmonic and quantum information fields. More recently, quantum statistical property of single plasmon was verified with metallic stripe waveguides<sup>18</sup> and bosonic nature of it was also proved in on-chip Hong-Ou-Mandel experiments<sup>19-22</sup> based on plasmonic waveguides, which show us the feasibility of achieving basic quantum logic gates for linear optical quantum computation. However, the excitation of SPPs is polarization-dependent, which may be an obstacle in the way of transmitting polarization entanglement in plasmonic waveguide. It is still unknown and remains as an experimental challenge whether quantum polarization entanglement can be maintained at the nanoscale plasmonic waveguides. Fortunately, a free-standing silver nanowire may be a good candidate to answer this question, since it supports not only the fundamental mode, but also two orthogonal higher-order modes that can match the polarization of

photons (see the Supporting information), which outperforms the widely studied dielectric-loaded SPP waveguide<sup>23</sup> and the metal strip waveguide,<sup>24</sup> for which SPPs can only be excited with transverse magnetic (TM) mode light.

In this work, we studied the transmission of a photonic quantum-entangled state through a nanoscale hybrid plasmonic waveguide, composed of a silica tapered fiber and a silver nanowire. By performing quantum state tomography<sup>25</sup> and a CHSH inequality test, preservation of the quantum polarization entanglement in the waveguide is demonstrated unambiguously, pushing the way forward to utilize quantum polarization entanglement in plasmonic field. Importantly, this quantum entanglement-maintaining nano-scale waveguide is fiber integrated, highly efficient, broadband, robust and free to move. Therefore, it is a perfect candidate to be used as near-field quantum probe for NSOMs and endoscopes,<sup>26,27</sup> and may also be useful for quantum photonic integrated circuits.<sup>22,28,29</sup>

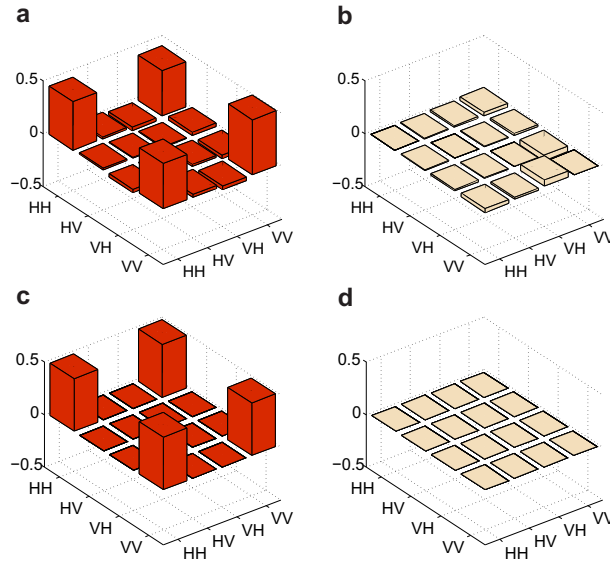


Figure 2: (color online) Density matrix of the output state from the fiber taper and  $\Phi^+$ . (a) and (b) Real and imaginary parts of the density matrix of the output state from the fiber taper. (c) and (d) Real and imaginary parts of the density matrix of  $\Phi^+$ .

# Experiment and Results

In our experiment, the polarization entangled two-photon state

$$\Phi^+ = \frac{1}{\sqrt{2}}(|HH\rangle + |VV\rangle), \quad (1)$$

was used to investigate the preservation of the quantum entanglement in nanoscale waveguides.  $\Phi^+$  is a maximally polarization entangled Bell state, where  $H(V)$  denotes horizontal (vertical) polarization. The entangled photon pairs were generated via a type-I spontaneous parametric down conversion (SPDC) process as depicted in Figure 1(a). The generated quantum state was characterized by quantum state tomography (Figure 1(b)). The concurrence<sup>30</sup> of the measured density matrix was 0.924 (it is 1 for a maximally entangled state and 0 for non-entangled state), and has a fidelity of 0.976 with the ideal state  $\Phi^+$  (see the Supporting information).

To excite SPPs on the silver nanowire efficiently and make the nanowire free-standing, we used a fiber taper<sup>31</sup> to connect and lift the silver nanowire. As shown in Figure 1(c), the taper has a very smooth surface, and the diameter is adiabatically decreased from 125  $\mu m$  to about 120 nm with a cone angle of about 3.5°. Therefore, the photons in fiber can be adiabatically focused into the nanoscale taper tip with negligible loss. Due to the perfect cylindrical symmetry of the taper, the polarization of the photons should be preserved during the focusing process. The maintaining of the quantum entanglement through the taper was verified firstly by sending one of the two entangled photons into the tapered fiber and the other through a single mode fiber, as illustrated in Figure 1(b). The re-radiated photon from the fiber taper was collected using an objective lens ( $NA = 0.8$ ), and a confocal system composed of two lenses and one pinhole. The pinhole was used to block the scattered background light and enhance the signal to noise ratio. The quantum correlation between the two photons was then investigated by quantum state tomography. The real and imaginary parts of the measured density matrix are shown in Figure 2(a) and 2(b), and exhibit good agreement with the corresponding parts of  $\Phi^+$  (Figure 2(c) and 2(d)). Further calculations showed that the quantum concurrence was 0.852 and the fidelity of the output state with  $\Phi^+$  was

0.958.

Additionally, CHSH inequality tests were performed to examine the non-local feature of the output photons. A hidden variable model requires that

$$|S| = |E(\hat{A}_1, \hat{B}_1) - E(\hat{A}_1, \hat{B}_2) + E(\hat{A}_2, \hat{B}_1) + E(\hat{A}_2, \hat{B}_2)| \leq 2, \quad (2)$$

where  $E(\hat{A}_i, \hat{B}_j)$  ( $i, j = 1, 2$ ) is the expectation value of operator  $\hat{A}_i \hat{B}_j$ , and  $\hat{A}_i$  and  $\hat{B}_j$  are the measurement operators on the two photons, respectively.  $\hat{A}_1$ ,  $\hat{B}_1$ ,  $\hat{A}_2$  and  $\hat{B}_2$  correspond to  $|H\rangle\langle H|$ ,  $|A\rangle\langle A|$ ,  $|V\rangle\langle V|$  and  $|D\rangle\langle D|$ , respectively, while  $|A\rangle$  denotes  $\frac{1}{\sqrt{2}}(|H\rangle + |V\rangle)$ ,  $|D\rangle$  denotes  $\frac{1}{\sqrt{2}}(|H\rangle - |V\rangle)$  (see the Supporting information for detail). The maximal value of  $S$  in our experiment was  $2.588 \pm 0.141$ , which definitely violates the hidden variable model. This further confirmed that the output photons were still entangled after emerging from the taper.

A fiber taper is unique for the efficient coupling with other photonic micro/nano-structures, because of the strong evanescent field around the taper (see the Supporting information). Therefore, it is natural to hybridize this dielectric waveguide with a SPP nano-structure. Here, a silver nanowire was adopted. As shown in Figure 1(c) and 1(d), the silver nanowire was adhered to the tip of the fiber taper, and the coupling efficiency was high. In addition to the nano-scale photonic confinement, there are several other benefits from such a hybrid dielectric-metal nanotip: (1) Compactness. The highly efficient light coupling between the silica taper and silver nanowire can be achieved within the wavelength scale coupling region, avoiding harmful absorption loss in metal.<sup>32,33</sup> (2) In-line geometry. Photons from a single mode fiber can be efficiently focused onto the tip of the silver nanowire. The transmission coupling efficiency from the fiber to the silver nanowire was estimated to be as high as 40% in our experiment. (3) Robustness. The structure is very robust and free to move; therefore, it has the potential to be used in a quantum endoscope.<sup>26,27</sup>

Before testing the preservation of the quantum entanglement, we first investigated the transmission of the hybrid tip using single photons. The reason for doing so was that the coupling between the fiber taper and the silver nanowire was a two-mode to three-mode process (see the Supporting

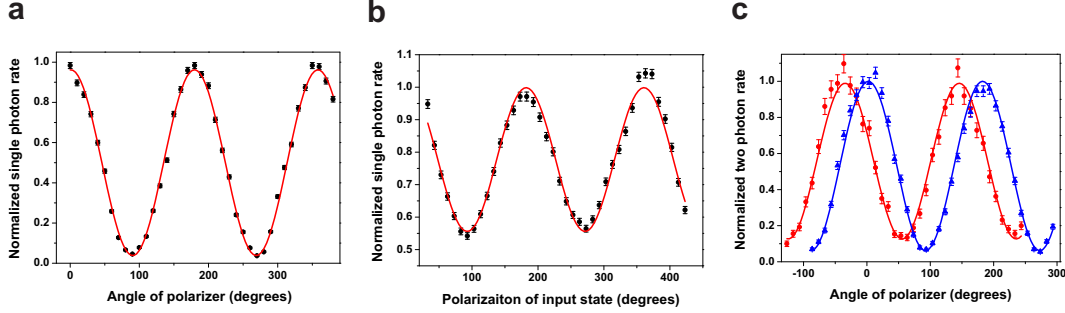


Figure 3: (color online) Single and biphoton fringes for the case of the silver nanowire. The points are experimentally measured data and are fitted with a sinusoidal function. (a) Single photon polarization property of the fiber-nanowire structure. After injecting horizontally-polarized photons, we measured the output counts while changing the orientation of the polarizer in steps of  $10^\circ$ , where  $0^\circ$  corresponds to measurement of the  $H$  state. (b) Transmission property of the fiber-nanowire structure for different linearly polarized photons. We measured the output counts while changing the polarization of the input photons in steps of  $10^\circ$ , where  $0^\circ$  denotes the  $H$  state. (c) Biphoton fringes corresponding to fourth-order quantum interference. Blue and red dots are coincidence rates when one photon was projected to a different polarization state, while the other is projected to the  $H$  and  $\frac{1}{\sqrt{2}}(|H\rangle + |V\rangle)$  states, respectively. Error bars are calculated from Poissonian statistics.

information), and the contact region of the silver nanowire and the silica fiber tip was not cylindrically symmetric (see Figure 1(d)), which influences the coupling between the dielectric waveguide mode and the SPPs. First,  $H$ -polarized single photons were sent into the hybrid tip, and the polarization of the transmitted photons were analyzed by a half wave plate (HWP) and a polarizer. The results are shown in Figure 3(a). The extinction ratio was measured to be 25 : 1, which indicates that the  $H$ -polarization was preserved throughout the entire process (propagation of the photons in the silica fiber, adiabatic focusing of the photons in the taper, conversion between the photons and plasmons, propagation of the plasmons in the silver nanowire, and scattering of the plasmons into free space photons at the end of the nanowire). Secondly, the coupling efficiencies for photons with different polarization were measured (Figure 3(b)). Due to the asymmetric structure in the contact area, the coupling efficiency changed with the polarization of the input photons and the ratio between the  $H$  and  $V$  polarized photons was approximately 1.78, close to the calculated result of 1.59 (see the Supporting information). The oscillations in the curve will be eliminated if the coupling efficiency is identical for  $H$  and  $V$  polarized photons.

Entangled photons were then used to test the hybrid tip, using an experimental set-up simi-



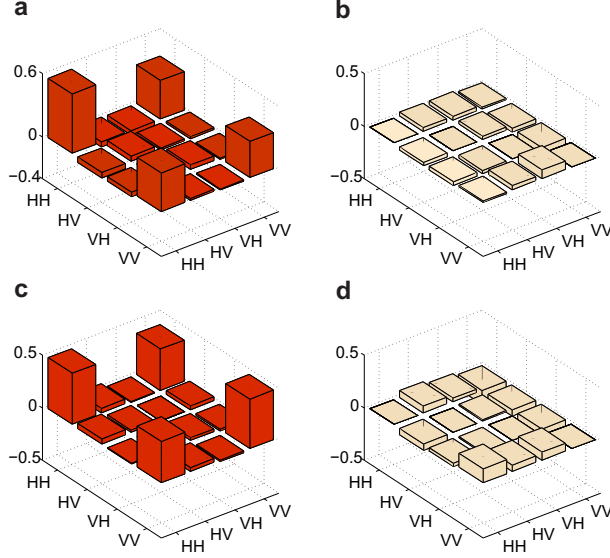


Figure 4: (color online) Density matrix of the output state for the case of the silver nanowire. (a) and (b) Real and imaginary parts of the density matrix of the original state from the silver nanowire. (c) and (d) Real and imaginary parts of the density matrix of the output state after an operation on the polarization of the pump laser to compensate the unbalanced efficiencies of different polarizations. The output state has a fidelity of 0.932 with the maximally entangled state  $\Phi^+$ .

lar to that used for the fiber taper. To show the entanglement of the output photons intuitively, we measured the coincidence rate by projecting one photon to a fixed state, while scanning the projection state of the other. If the photons are entangled, we can always find special projection states to make the coincidence be 0. For example, for the maximally entangled state  $\Phi^+$ , when one photon is projected to  $|D\rangle = \frac{1}{\sqrt{2}}(|H\rangle + |V\rangle)$ , the other photon will be correspondingly collapsed to  $|D\rangle$ . Therefore, the coincidence rate will become 0 when we measure the other photon using the  $\frac{1}{\sqrt{2}}(|H\rangle - |V\rangle)$  basis. Similarly, if we project the first photon to state  $|H\rangle$ , the coincidence rate will become 0 with the other measured basis as  $|V\rangle$ . The experimental biphoton fringes are shown in Figure 3(c), which can be treated as intuitive evidence of entanglement. Furthermore, QST and CHSH inequality tests were also performed. The density matrix is shown in Figure 4(a) and 4(b). It has a concurrence of 0.700 and a fidelity of 0.924 with the eigenstate  $\tilde{\Phi} = 0.801|HH\rangle + 0.594|VV\rangle$ , which was calculated using the density matrix diagonalization method. Therefore, we can consider  $\tilde{\Phi}$  approximately to be the output state. The change of state from the initial state to non-maximally entangled state  $\tilde{\Phi}$  came from the unbalanced coupling efficiency of the  $H$  and  $V$  photons, which

was consistent with the measured value 1.78 for single photons. To compensate the unbalanced coupling efficiencies, we can adjust the ratio between  $|HH\rangle$  and  $|VV\rangle$  of the input state by changing the polarization of the pump laser. In this way, the output state could be tuned to the maximally entangled state  $\Phi^+$ , with a fidelity of 0.932 and a concurrence of 0.824 (Figure 4(c) and 4(d)). The parameter of the CHSH inequality was  $2.495 \pm 0.147$ , indicating violation of the hidden variable theory.

## Discussion

In plasmonic experiments, loss has long been considered to be the major roadblock for practical applications. Here, we give a brief discussion on whether loss would influence the entanglement. In our experiment, three processes are responsible for the losses: the coupling between the fiber taper and the silver nanowire, the intrinsic loss of the plasmonic modes when propagating along the nanowire and non-unity collection efficiency. Due to the symmetric shape of the silver nanowire, the two higher-order modes of the structure used in our experiment are degenerate, thus they experience the same loss in the propagation process. The same as the absorption of the metal nanowire, the collection process is also polarization independent, so both of the two processes have no influence on the polarization entanglement. While as mentioned above, the fiber-nanowire coupling process is polarization dependent, because the coupling region is asymmetric for two different polarizations. Thus the input polarization state will be changed to a non-maximally entangled state. Fortunately, this problem can be settled by adjusting the input entangled state or the collection equipment to ensure that the output photons are still maximally entangled as shown in Figure 4(c) and 4(d).

In our experiment, the total transmittance from the photon source to the detector was about 7.5% for  $H$ -polarized photons. Taking into account of the collection efficiency of the objective lens, the efficiency of the confocal system and the free-space-to-fiber coupling efficiency (about 40.1%, 70.5% and 70.2%, respectively), the efficiency from the fiber taper to the silver nanowire

is estimated to be about 40.3% (see the Supporting information). By adjusting the shape of the fiber taper and the coupling length, this efficiency can be improved to even higher than 90%.<sup>34</sup> Compared to general near field probes, this high efficiency provides us an opportunity to extract and study weak signals in the near field. In addition, the effective mode area of the silver nanowire was only about  $0.38\lambda^2$ , corresponding to a spot with diameter of  $0.35\lambda$  (see the Supporting information). This mode area can be much smaller if we use the fundamental mode.<sup>35</sup>

In summary, we have experimentally realized the transmission of quantum polarization entanglement in a hybrid nanoscale plasmonic waveguide. This hybrid device can confine the effective mode area to subwavelength scale and can be applied as a quantum probe to realize high spatial resolution and highly sensitive measurements, or to perform remote excitation and remote sensing with the help of quantum entanglement,<sup>36</sup> and the high efficiency of the device makes these applications quite feasible. Our studies encourage further investigations of the quantum effect in nanostructures through the coupling of these waveguides, thus bridging free space quantum optical techniques and nanophotonics. For example, we can envision a quantum nanoscope that simultaneously beats the diffraction limit and SQL by using the techniques exploited here.

## **Supporting Information**

The Supporting Information contains the fabrication method of the silver nanowire and the fiber taper, a detailed description of quantum state tomography and CHSH test, the reconstructed density matrix of the entangled photon source and the numerical simulation of the modes and the transmission properties of our structure. This material is available free of charge via the Internet at <http://pubs.acs.org>.

## **Acknowledgement**

This work was funded by NBRP (grant nos. 2011CBA00200 and 2011CB921200), the "Strategic Priority Research Program(B)" of the Chinese Academy of Sciences(Grant No. XDB01030200),

NNSF (grant nos.11374289), the Fundamental Research Funds for the Central Universities (grant no, WK2470000012) and NCET. We thank Y. F. Huang, B. H. Liu, G. Y. Xiang, F. W. Sun, Z. B. Hou, W. Fang, H. K. Yu and H. Y. Zhang for useful discussion.

## Notes

The authors declare no competing financial interests .

## References

- (1) Horodecki, R.; Horodecki, P.; Horodecki, M.; Horodecki, K. *Rev. Mod. Phys.* **2009**, *81*, 865.
- (2) Bell, J. S. *Physics* **1964**, *1*, 195-200.
- (3) Clauser, J. F.; Horne, M. A.; Shimony, A.; Holt, R. A. *Phys. Rev. Lett.* **1969**, *23*, 880.
- (4) Giovannetti, V.; Lloyd, S.; Maccone, L. *Nat. Photonics* **2011**, *5*, 222-229.
- (5) Kuzmich, A.; Mandel, L. *Quant. Semiclass. Opt.* **1998**, *10*, 493-500.
- (6) Rarity, J.G.; Tapster, E.; Jakeman, E.; Larchuk, T.; Campos, R. A.; Teich, M. C.; Saleh, E. A. *Phys. Rev. Lett.* **1990**, *65*, 1348-1351.
- (7) Nagata, T.; Okamoto, R.; O'Brien, J. L.; Sasaki, K.; Takeuchi, S. *Science* **2007**, *316*, 726-729.
- (8) Xiang, G. Y.; Higgins, B. L.; Berry, D. W.; Wiseman, H. M.; Pryde, G. J. *Nat. Photon.* **2010**, *5*, 43-47.
- (9) Ono, T.; Okamoto, R.; Takeuchi, S. *Nat. Commun.* **2013**, *4*, 2426.
- (10) Israel, Y.; Rosen, S.; Silberberg, Y. *Phys. Rev. Lett.* **2014**, *112*, 103604.
- (11) Barnes, W. L.; Dereux, A.; Ebbesen, T. W. *Nature* **2003**, *424*, 824-830.
- (12) Ozbay, E. *Science* **2006**, *311*, 189-193.

- (13) Xiong, X.; Zou, C. L.; Ren, X. F.; Liu, A. P.; Ye, Y. X.; Sun, F. W.; Guo, G. C. *Laser Photonics Rev.* **2013**, *7*, 901-919.
- (14) Guo, X.; Ma, Y. G.; Wang, Y. P.; Tong, L. M. *Laser Photonics Rev.* **2013**, *7*, 855-881.
- (15) Altewischer, E.; Van Exter M. P.; Woerdman, J. P. *Nature* **2002**, *418*, 304-306.
- (16) Fasel, S.; Robin, F.; Moreno, E.; Erni, D.; Gisin, N.; Zbinden, H. *Phys. Rev. Lett.* **2005**, *94*, 110501.
- (17) Ren, X. F.; Guo, G. P.; Huang, Y. F.; Li, C. F.; Guo, G. C. *Europhys. Lett.* **2006**, *76*, 753.
- (18) Martino, G. D.; Sonnefraud, Y.; Kéna-Cohen, S.; Tame, M.; Özdemir, S. K.; Kim, M. S.; Maier, S. A. *Nano Lett.* **2012**, *12*, 2504-2508.
- (19) Heeres, R. W.; Kouwenhoven, L. P.; Zwiller, V. *Nat. Nanotech.* **2013**, *8*, 719-722.
- (20) Fakonas, J. S.; Lee, H.; Kelaita, Y. A.; Atwater, H. A. *Nat. Photon.* **2014**, *8*, 317-320.
- (21) Martino, G. D.; Sonnefraud, Y.; Tame, M. S.; Kéna-Cohen, S.; Dieleman, F.; Özdemir, S. K.; Kim, M. S.; Maier, S. A. *Phy. Rev. Applied* **2014**, *1*, 034004.
- (22) Cai, Y. J.; Li, M.; Ren, X. F.; Zou, C. L.; Xiong, X.; Lei, H. L.; Liu, B. H.; Guo, G. P.; Guo, G. C. *Phys. Rev. Applied* **2014**, *2*, 014004.
- (23) Kumar, A.; Gosciniak, J.; Volkov, V. S.; Papaioannou, S.; Kalavrouziotis, D.; Cyrsoinos, K.; Weeber, J. C.; Hassan, K.; Markey, L.; Dereux, A.; Tekin, T.; Waldow, M.; Apostolopoulos, D.; Pleros, N.; Bozhevolnyi, S. I. *Laser Photonics Rev.* **2013**, *7*, 938-951.
- (24) Derigon, A.; Smith, D. *Opt. Express* **2006**, *14*, 1611-1625.
- (25) James, D. F. V.; Kwiat, P. G.; Munro, W. J.; White, A. G. *Phys. Rev. A* **2001**, *64*, 052-312.
- (26) Yan, R. X.; Park, J. H.; Choi, Y.; Heo, C. J.; Yang, S. M.; Lee, L. P.; Yang, P. D. *Nat. Nanotech.* **2012**, *7*, 191-196.

- (27) Lu, G.; De, K. H.; Su, L.; Kenens, B.; Rocha, S.; Fron, E.; Chen, C.; Van, D. P.; Mizuno, H.; Hofkens, J.; Hutchison, J.; Uji-i, H. *Adv. Mater.* **2014**, *26*, 5124-5128.
- (28) Wei, H.; Wang, Z. X.; Tian, X. R.; Kall, M.; Xu H. X., *Nat. Commun.* **2011**, *2*, 387.
- (29) Politi, A.; Matthews, J.; Thompson, M.; O'Brien, J. *IEEE J. Sel. Top. Quant. Electron.* **2009**, *15*, 1673-1684.
- (30) Hill, S.; Wootters, W. K. *Phys. Rev. Lett.* **1997**, *78*, 5022.
- (31) Wu, X. Q.; Tong, L. M. *Nanophotonics* **2013**, *2*, 407-428.
- (32) Dong, C. H.; Ren, X. F.; Yang, R.; Duan, J. Y.; Guo, G. P.; Guo, G. C. *Appl. Phys. Lett.* **2009**, *95*, 221109.
- (33) Guo, X.; Qiu, M.; Bao, J. M.; Wiley, B. J.; Yang, Q.; Zhang, X. N.; Ma, Y. G.; Yu, H. K.; Tong, L. M. *Nano Lett.* **2009**, *9*, 4515-4519.
- (34) Li, X. Y.; Li, W.; Guo, X.; Lou, J. Y.; Tong, L. M. *Opt. Express* **2013**, *21*, 15698-15705.
- (35) Wang, Y. P.; Ma, Y. G.; Guo, X.; Tong L. M. *Opt. Express* **2012**, *20*, 19006-19015.
- (36) Ren, X. F.; Guo, G. P.; Huang, Y. F.; Wang, Z. W.; Zhang, P.; Guo, G. C. *Europhys. Lett.* **2008**, *84*, 30005.